

Tumbling of Inertial Fibers in Turbulence

S. Bounoua,^{1,2} G. Bouchet,² and G. Verhille^{1,*}

¹*Aix Marseille Univ, CNRS, Centrale Marseille, IRPHE, F-13013 Marseille, France*

²*Aix Marseille Univ, CNRS, IUSTI, F-13013 Marseille, France*



(Received 23 April 2018; published 20 September 2018)

Anisotropic particles play a major role in many environmental and industrial turbulent flows. The modeling of their rotation dynamics is a fundamental challenge which has some important consequences in industrial processes, such as in the paper making industry. This study investigates the rotation rate of neutrally buoyant fibers longer than the Kolmogorov length η_K . We show that the fiber inertia is at the origin of a decrease of the rotation rate. We propose a model which describes this phenomenon. We introduce also a new Stokes number which defines the limit of validity of the classical slender body approximation.

DOI: 10.1103/PhysRevLett.121.124502

The rotational dynamics of fiberlike particles in turbulence is a key feature for both fundamental and applied sciences. For instance, in environmental sciences, the chemotaxis of planktons, which play a major role in the carbon budget in the ocean, depends on the rotation rate of the organisms [1]. In industrial flows, the quality of the paper depends on the fiber orientation in the sheet. This orientation is determined by the hydrodynamical processes during the paper making [2]. Moreover, it has been shown that the orientation dynamics of small neutrally buoyant fiber is strongly correlated to the local vorticity of the flow, opening new perspectives to probe the properties of turbulence [3].

For an axisymmetric particle, the rotation dynamics can be decomposed into two modes: the spinning, which corresponds to the rotation around the axis of symmetry \mathbf{p} of the particle, and the tumbling which corresponds to the rotation of this axis of symmetry [4]. There are few studies on the spinning of spheres in turbulence [5–7]. However, most of the studies on the rotation of particles focus on the tumbling of anisotropic particles [8–12]. Experimental works on fibers smaller than the Kolmogorov length $\eta_K = (\nu^3/\epsilon)^{1/4}$ [8–10], where ν is the kinematic viscosity of the fluid and ϵ the dissipation rate of the turbulent kinetic energy, are in good agreement with numerical and theoretical predictions: the dynamics is determined by a preferential alignment of the particle with the local vorticity [3,13]. For fiber longer than the Kolmogorov length, currently there are only two different studies which find different results. In the first one [12], they used thin fibers with diameter d smaller than or equal to η_K . Varying the fiber length L , they found that the tumbling rate $\langle \dot{p}_i \dot{p}_i \rangle$ scales as $(L/\eta_K)^{-4/3}$ independent of the aspect ratio of the particle. This prediction is in agreement with slender body (SB) prediction [14,15] for which the fiber inertia is

neglected when its aspect ratio $\Lambda = L/d$ is large enough ($\Lambda \gg 1$) as “the volume of fluid set in motion by the translation and rotation of a fibre is a sphere of diameter L , the fluid inertia is much more important than the inertia of the fiber itself” [15]. In the second one [11], they used large fibers ($d > \eta_K$ and $L > \eta_K$) and focused on the total rotation (tumbling + spinning) rate $\langle \Omega_i \Omega_i \rangle$. They found that the rotation rate scales as $\langle \Omega_i \Omega_i \rangle \sim (d_{\text{eq}}/\eta_K)^{-4/3}$ where $d_{\text{eq}}^3 = Ld^2$ is a characteristic length defined from the volume of the fiber. This experimental law can be written as $\langle \Omega_i \Omega_i \rangle \sim \Lambda^{8/3} (L/\eta_K)^{-4/3}$. This suggests that for a given length L the rotation of the fiber should increase as the diameter decreases. To understand the role of the particle aspect ratio and the difference between these two studies, we have studied the tumbling rate of fibers varying independently the length L and the diameter d of the fibers. From our measurements we derived a model underlying the role of the fiber inertia which allows to collapse the three studies on a master curve.

The experiments are performed within a cubic tank of 60 cm of side filled with water. The turbulence is generated by the rotation of 8 disks, one at each corner, of 17 cm in diameter fitted with blades. The impellers are set independently into motion with 1.5 kW brushless motor. Here, all the disks rotate at the same frequency F but in opposite direction, cf. Fig. 1. The turbulence has been characterized by classical two-dimensional particle image velocimetry (2D PIV) [16,17] and the main characteristics are given in Table I. The rigid fibers are cut at the desired length L from polystyrene rod with a diameter d varying between 500 μm and 2.5 mm. Here, the length varies from 3.2 to 40 mm leading to aspect ratio Λ between 2.5 and 80. Higher aspect ratio was not tested to avoid fiber deformations due to turbulent fluctuations [18]. The concentration of fibers is always very small (less than 0.01%) so the interaction

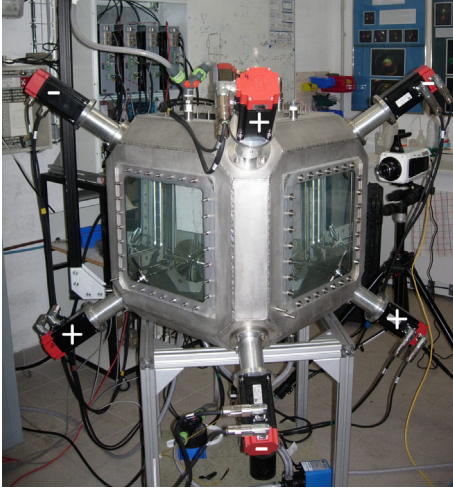


FIG. 1. The cube facility. The motor tagged with a + (respectively, -) rotates in clockwise (respectively, counterclockwise) direction.

between fibers and their action on the turbulence can be neglected. The density of the polystyrene is $\rho = 1.04$ so buoyancy forces are negligible compared to hydrodynamical forces.

Two 1 MP high speed cameras are used to image the particles at a frame rate of 500 or 1000 frames/s depending on the impeller rotation frequency F . The light is produced by a LED panel placed in front of each camera (back lighting). The 3D reconstruction is performed with MATLAB in two steps. First, the extremities of each fiber are determined on each of the images and triangulated. Then, an optimization is performed on the position and the orientation of each fiber to minimize the distance between the projection of the reconstructed particle and the edges of the fiber on each image. An example of trajectory is presented in Fig. 2. The volume of reconstruction is approximately a cube of ~ 13 cm in length centered on the center of the device. 2D PIV measurements in the midplane of this volume show that the turbulence is homogeneous and isotropic in a good approximation. At least five thousand of the trajectories are then stored and used to compute the rotation statistics. Here, we focus on the evolution of the variance of the tumbling rate $\langle \dot{p}_i \dot{p}_i \rangle$, where $\langle \cdot \rangle$ corresponds to a time and ensemble average. To get rid of the experimental noise, the variance is estimated by the technique proposed by [19,20]. The signal $\mathbf{p}(t)$ is filtered with a Gaussian filter of width σ_G . The variance of the filtered signal is computed for each case and the

TABLE I. Characteristics of the turbulence in the cube facility.

Rotation frequency F	5–15 Hz
Reynolds number R_λ	350–610
Integral scale L_I	6 cm
Taylor microscale $\lambda = \sqrt{15/\nu\epsilon}u_{rms}^2$	1.5–2.5 mm
Kolmogorov length η_K	34–78 μm

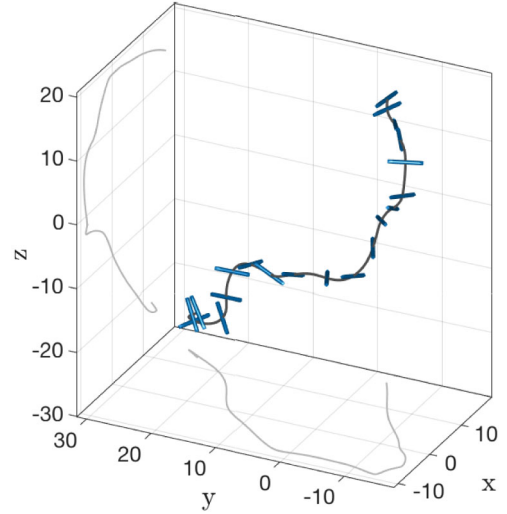


FIG. 2. Example of trajectory reconstructed in the cube for a fiber with a diameter of $650 \mu\text{m}$ and a length of 10 mm. The axis units are in mm (the particle is not at scale) and this trajectory last more than 20 turnover time.

tumbling rate $\langle \dot{p}_i \dot{p}_i \rangle$ is determined by extrapolating the value for $\sigma_G = 0$.

We test on Fig. 3 the two predictions from the two previous studies. The main figure shows the evolution of the tumbling rate as a function of the fiber length L . As one can see the global behavior of the measurements is relatively well described by the SB prediction for fibers with random orientation given in [12] [$\langle \dot{p}_i \dot{p}_i \rangle \sim (L/\eta_K)^{-4/3}$]. However, our measurements are always smaller than the prediction and this difference increases with the Reynolds number R_λ . This suggests that the normalization by the Kolmogorov time $\tau_K = (\nu/\epsilon)^{1/2}$ and the Kolmogorov length η_K does not capture all the physics of this problem. The inset represents the evolution of the tumbling rate as a function of the equivalent diameter d_{eq} proposed by [11]. As one can see the scattering is larger than for the previous case and the global behavior is not captured by this model.

To understand the scattering of the experimental points, we will derive a model close to the SB approximation but taking into account the fiber inertia. In the frame of the fiber the conservation of the kinetic momentum is given by

$$I\dot{\Omega} + \Omega \times (I \cdot \Omega) = \Gamma, \quad (1)$$

where I is the moment of inertia tensor, Ω the rotation rate of the fiber, $\dot{\Omega}$ its derivative with time, and Γ is the torque applied on the particle [4]. The maximal Reynolds number based on the fiber diameter $\text{Re}_d \sim (d/\eta_K)^{4/3}$ [21] is of the order of 300. Even if this value is relatively high, we will assume that the torque is a viscous torque (linear in velocity) and not a turbulent torque (proportional to the square of the velocity) [22]. Then, in first approximation, the torque is given by $\Gamma = \int 4\pi\eta \mathbf{u}_s \times \mathbf{s} ds$, with \mathbf{u}_s the slip

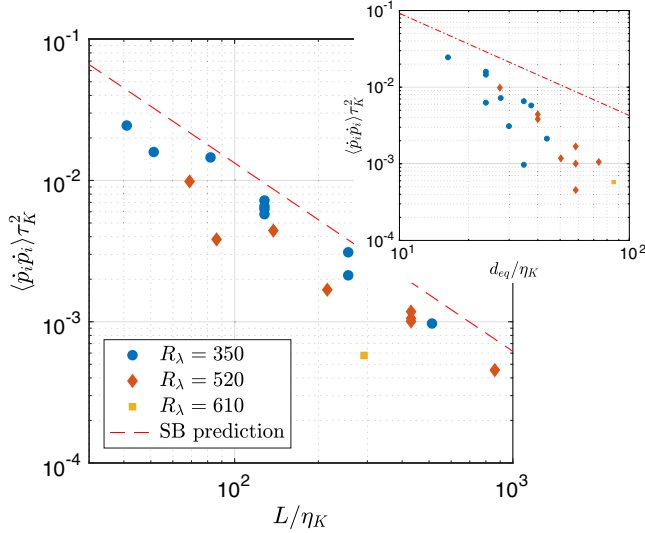


FIG. 3. The main figure represents the evolution of the variance of the tumbling rate as a function of the fiber length for the different particle tested here. The dashed line represents the SB prediction [12]. In the inset, the tumbling rate is plotted as a function of the equivalent diameter d_{eq} , the dot-dashed line represents the prediction done in [11].

velocity and s the curvilinear coordinate with $s = 0$ at the center of the fiber and η the dynamical viscosity of the fluid. Note that rigorously, the viscosity η should be replaced by a tensor with different values for the parallel and the perpendicular components of the slipping velocity. However, this anisotropy should not play a major role here, as only the perpendicular component is concerned for the torque, and will be neglected here such as the logarithmic correction [23]. In the fiber frame, the slip velocity scales as $\mathbf{u}_s \sim (\mathbf{u}_f - s \times \boldsymbol{\Omega})$ where \mathbf{u}_f is the fluid velocity, and so, the torque as $\boldsymbol{\Gamma} \sim -4\pi\eta L^3 \boldsymbol{\Omega}/3 + 4\pi\eta \int \mathbf{u}_f \times s ds$. The fluid velocity \mathbf{u}_f is a noise with spatiotemporal correlation. However, a scale selection occur with the integral. Hence, the scales smaller than the fiber length do not contribute to the torque as they are not correlated on the fiber length. Similarly, the large scales do not contribute for the rotation either as the velocity is homogeneous at the scale of the fiber (they should only contribute to the translation). Therefore, the viscous torque at the origin of the tumbling can be approximated by

$$\boldsymbol{\Gamma} \sim -\frac{4\pi}{3}\eta L^3 \boldsymbol{\Omega}_t + 4\pi\eta L^2 u_L, \quad (2)$$

where $\boldsymbol{\Omega}_t$ is the tumbling rate ($\dot{\mathbf{p}} = \boldsymbol{\Omega}_t \times \mathbf{p}$) and $u_L \sim (\epsilon L)^{1/3}$ is the typical velocity at scale L . Note that the scaling $\langle \dot{p}_i \dot{p}_i \rangle \sim (L/\eta_K)^{-4/3}$ is derived from this expression. As the fiber inertia is neglected for the classical slender body approximation ($I = 0$), the torque vanishes $\boldsymbol{\Gamma} = 0$. So, $\langle \dot{p}_i \dot{p}_i \rangle \sim (u_L/L)^2 \sim (L/\eta_K)^{-4/3}$. In our model, the fiber inertia is taken into account ($I \neq 0$) but not the

Coriolis term $\boldsymbol{\Omega} \times (I \cdot \boldsymbol{\Omega})$. Considering the tumbling, this nonlinear term can be written $I_t \boldsymbol{\Omega}_t \boldsymbol{\Omega}_s$, where $\boldsymbol{\Omega}_s$ is the spinning rate and I_t the moment of inertia of the fiber for the tumbling [$I_t = m(3d^2/4 + L^2)/12$ for a homogeneous fiber of mass m , length L , and diameter d]. Neglecting the Coriolis term is then valid if the spinning rate is small compared to the characteristic time of evolution of the tumbling rate $\tau_r \sim I_t/4\pi\eta L^3$ ($\boldsymbol{\Omega}_s \tau_r \ll 1$), defined by the ratio of the inertial term $I\boldsymbol{\Omega}$ and the viscous term $4\pi\eta L^3 \boldsymbol{\Omega}$. We will discuss this assumption in the conclusion of the Letter.

With these different assumptions, the evolution of the tumbling rate can be written

$$\dot{\boldsymbol{\Omega}}_t + \frac{1}{\tau_r} \boldsymbol{\Omega}_t = \frac{1}{\tau_r} \frac{u_L}{L}. \quad (3)$$

This equation is a Langevin equation excited by a colored noise $\xi = u_L/L$ and with a response time τ_r . This equation shows that the fiber acts as a lowpass filter for the turbulent fluctuations. The variance of the tumbling rate is then directly given by the spectrum of the excitation $|\xi(\omega)|^2$:

$$\langle \boldsymbol{\Omega}_t \boldsymbol{\Omega}_t \rangle = \int \left| \frac{1}{1 + i\tau_r \omega} \right|^2 |\xi(\omega)|^2 d\omega. \quad (4)$$

Currently, there is no theoretical prediction for the spectrum $\xi(\omega)$. As ξ is a colored noise with a characteristic time $\tau_L = L/u_L$, the spectrum should be peaked around the frequency $\omega_L = 1/\tau_L$. Hence, in the first approximation, the spectrum can be approximated by a Dirac function $\xi(\omega) = \epsilon^{1/3} L^{-2/3} \delta(\omega - \omega_L)$. Then, the tumbling rate is given by

$$\langle \boldsymbol{\Omega}_t \boldsymbol{\Omega}_t \rangle \sim \frac{1}{1 + St_t^2} \tau_K^{-2} \left(\frac{\eta_K}{L} \right)^{4/3}, \quad (5)$$

with $St_t = \omega_L \tau_r$ defining a tumbling Stokes number, comparing the forcing timescale τ_L , and the relaxation timescale of the tumbling rate τ_r . For $St_t \ll 1$, Eq. (5) is similar to the SB prediction, whereas for $St_t \gg 1$, the variance of the tumbling rate is smaller than the SB prediction as the forcing evolves on a timescale much smaller than the response time of the fiber. For a cylindrical fiber of diameter d , length L , and density ρ , the tumbling Stokes number is equal to

$$St_t = \frac{1}{48} \frac{\rho}{\rho_f} \left(\frac{d}{\eta_K} \right)^{4/3} \left(\frac{d}{L} \right)^{2/3} \left[1 + \frac{3}{4} \left(\frac{d}{L} \right)^2 \right], \quad (6)$$

where ρ_f is the fluid density. For a given η_K and d , the tumbling Stokes number decreases when the fiber length increases. This corresponds to the classical intuition that for a slender body the fiber inertia is negligible [15]. This phenomenon is directly related to the forcing timescale

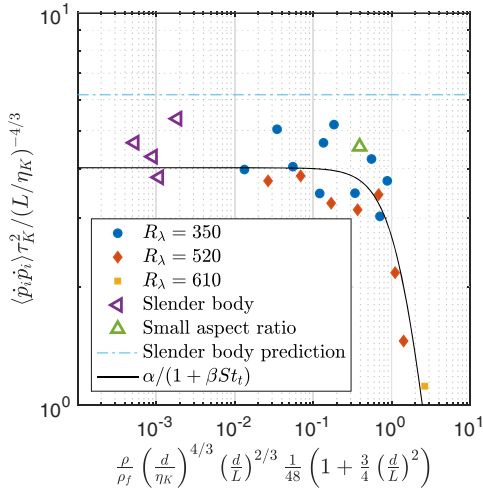


FIG. 4. Evolution of the transfer function as a function of the tumbling Stokes number St_t for the all the different experimental measurements of the tumbling rate: [12] (triangle left), [11] (triangle), and this study (plain symbol). The line corresponds to the best fit of our results of Eq. (5).

which decreases when L increases $\tau_L \sim L^{-2/3}$, whereas the tumbling timescale is independent of L . On the contrary, for a given L , St_t increases with the fiber diameter as the response time of the particle increases with the fiber diameter ($\tau_r \sim d^2$), whereas the forcing timescale is independent of d . Figure 4 represents the evolution of the normalized variance of the tumbling rate $\langle \dot{p}_i \dot{p}_i \rangle / \tau_K^{-2} (\eta_K/L)^{4/3}$ as a function of the rotational Stokes number St_t . One can see that our measurements and the ones of the literature [11,12] follow the same master curve and they are well fitted by the transfer function given in Eq. (5) (plain line on Fig. 4). This observation validates our different assumptions: mainly the Coriolis term can indeed be neglected and the viscous torque assumption hold even for the largest diameter used here. The plateau at low St_t corresponds to the domain of validity of the slender body theory. The amplitude found here is $\sim 30\%$ smaller than the prediction of the SB model for fibers with random orientation [12].

In conclusion, we studied experimentally the tumbling rate of fibers with various aspect ratio and various length in turbulence. We have introduced a new tumbling Stokes number St_t which characterizes the tumbling rate of a fiber. For low St_t the slender body approximation is valid and the tumbling rate evolves as $(L/\eta_K)^{-4/3}$. For high St_t the particle inertia cannot be neglected anymore and is at the origin of a filtering of the turbulent fluctuations and so to a reduction of the rotation rate. To fully characterize the rotation of rigid fiber in turbulent flows several questions still need to be investigated. First, it is known that fiber smaller than the Kolmogorov scale spins more than tumbles [4]. From our modeling, the net torque for the spinning is null for random orientation as the increments of velocity at the scale of the diameter u_d are not correlated at the scale of

the fiber length L . Therefore, the spinning might be a tool to probe the preferential alignment of inertial fibers in turbulence. Then, the statistics (probability density function and correlation function) of the rotation and the translation should be investigated. At a low Stokes number, measuring these different quantities might be used to investigate the inertial range of turbulence especially the coarse grained velocity gradient tensor.

This work was carried out in the framework of FlexFiT Project (ANR-17-CE30-0005-01) funded by the French National Research Agency (ANR), the Labex MEC Project (No. ANR-10-LABX-0092) and of the A*MIDEX Project (No. ANR-11-IDEX-0001-02), funded by the Investissements d'Avenir French Government program managed by the French National Research Agency (ANR).

*Corresponding author.

gautier.verhille@irphe.univ-mrs.fr

- [1] J. Guasto, R. Rusconi, and R. Stocker, Fluid mechanics of Planktonic microorganisms, *Annu. Rev. Fluid Mech.* **44**, 373 (2012).
- [2] F. Lundell, L. Söderberg, and P.H. Alfredsson, Fluid mechanics of papermaking, *Annu. Rev. Fluid Mech.* **43**, 195 (2011).
- [3] A. Pumir and M. Wilkinson, Orientation statistics of small particles in turbulence, *New J. Phys.* **13**, 093030 (2011).
- [4] G. Voth and A. Soldati, Anisotropic particles in turbulence, *Annu. Rev. Fluid Mech.* **49**, 249 (2017).
- [5] R. Zimmermann, Y. Gasteuil, M. Bourgoïn, R. Volk, A. Pumir, and J.-F. Pinton, Rotational Intermittency and Turbulence Induced Lift Experienced by Large Particles in a Turbulent Flow, *Phys. Rev. Lett.* **106**, 154501 (2011).
- [6] S. Klein, M. Gibert, A. Bérut, and E. Bodenschatz, Simultaneous 3D measurement of the translation and rotation of finite size particles and the flow field in a fully developed turbulent water flow, *Meas. Sci. Technol.* **24**, 024006 (2013).
- [7] V. Mathai, M. W. M. Neut, E. P. van der Poel, and C. Sun, Translational and rotational dynamics of a large buoyant sphere in turbulence, *Exp. Fluids* **57**, 51 (2016).
- [8] S. Parsa, E. Calzavarini, F. Toschi, and G. A. Voth, Rotation Rate of Rods in Turbulent Fluid Flow, *Phys. Rev. Lett.* **109**, 134501 (2012).
- [9] M. Byron, J. Einarsson, K. Gustavsson, G. Voth, B. Mehlig, and E. Variano, Shape-dependence of particle rotation in isotropic turbulence, *Phys. Fluids* **27**, 035101 (2015).
- [10] L. Sabban, A. Cohen, and R. van Hout, Temporally resolved measurements of heavy, rigid fibre translation and rotation in nearly homogeneous isotropic turbulence, *J. Fluid Mech.* **814**, 42 (2017).
- [11] A. D. Bordoloi and E. Variano, Rotational kinematics of large cylindrical particles in turbulence, *J. Fluid Mech.* **815**, 199 (2017).
- [12] S. Parsa and G. A. Voth, Inertial Range Scaling in Rotations of Long Rods in Turbulence, *Phys. Rev. Lett.* **112**, 024501 (2014).

- [13] K. Gustavsson, J. Jucha, A. Naso, E. L ev eque, A. Pumir, and B. Mehlig, Statistical Model for the Orientation of Nonspherical Particles Settling in Turbulence, *Phys. Rev. Lett.* **119**, 254501 (2017).
- [14] J. Olson and R. Kerekes, The motion of fibres in turbulent flow, *J. Fluid Mech.* **377**, 47 (1998).
- [15] M. Shin and D.L. Koch, Rotational and translational dispersion of fibres in isotropic turbulent flows, *J. Fluid Mech.* **540**, 143 (2005).
- [16] W. Thielicke and E. Stamhuis, PIVlab—towards user-friendly, affordable and accurate digital particle image velocimetry in MATLAB, *J. Open Res. Software* **2**, e30 (2014).
- [17] D. Xu and J. Chen, Accurate estimate of turbulent dissipation rate using PIV data, *Exp. Therm. Fluid. Sci.* **44**, 662 (2013).
- [18] C. Brouzet, G. Verhille, and P. Le Gal, Flexible Fiber in a Turbulent Flow: A Macroscopic Polymer, *Phys. Rev. Lett.* **112**, 074501 (2014).
- [19] N. Mordant, A. Crawford, and E. Bodenschatz, Experimental Lagrangian acceleration probability density function measurement, *Physica (Amsterdam)* **193D**, 245 (2004).
- [20] R. Volk, N. Mordant, G. Verhille, and J.-F. Pinton, Laser Doppler measurement of inertial particle and bubble accelerations in turbulence, *Europhys. Lett.* **81**, 34002 (2008).
- [21] M. Cisse, H. Homann, and J. Bec, Slipping motion of large neutrally buoyant particles in turbulence, *J. Fluid Mech.* **735**, R1 (2013).
- [22] M. Zastawny, G. Mallouppas, F. Zhao, and B. van Wachem, Derivation of drag and lift force and torque coefficients for non-spherical particles in flows, *Int. J. Multiphase Flow* **39**, 227 (2012).
- [23] E. Guazzelli, J. F. Morris, and S. Pic, *A Physical Introduction to Suspension Dynamics*, Cambridge Texts in Applied Mathematics (Cambridge University Press, Cambridge, 2011).